Carbon Consumption and Adsorption-Regeneration of H2S on Activated Carbon for Coke Oven Flue Gas Purification

Yuting Lin
Institute of Process Engineering Chinese Academy of Sciences
Yuran Li (yrli@ipe.ac.cn)
Institute of Process Engineering Chinese Academy of Sciences https://orcid.org/0000-0003-0131-9622
Zhicheng Xu
Institute of Process Engineering Chinese Academy of Sciences
Junxiang Guo
Institute of Process Engineering Chinese Academy of Sciences
Tingyu Zhu
Institute of Process Engineering Chinese Academy of Sciences

Research Article

Keywords: activated carbon, hydrogen sulfide, elemental sulfur, chemical carbon consumption, physical carbon abrasion

Posted Date: April 23rd, 2021

DOI: https://doi.org/10.21203/rs.3.rs-335006/v1

Abstract

Carbon consumption of activated carbon varies with the sulfur-containing products. In this work, differential thermogravimetric (DTG), electron paramagnetic resonance (ESR), X-ray photoelectron spectroscopy (XPS), and temperature programmed desorption (TPD) were used to reveal the adsorption-regeneration process of H 2 S and the effect of adsorption products on carbon consumption. H 2 S reacts with the C=C bond to form C-S bond as an intermediate state, followed by the formation of elemental sulfur. It directly sublimates at approximately 380 °C , about 30 °C higher than the decomposition temperature of H 2 SO 4 . In the thermal regeneration process, the elemental sulfur in the form of monoclinic sulfur (S 8) first breaks into infinitely long chain molecules (S ∞) and then into small molecules, finally into sulfur vapor. The desorption of elemental sulfur consumes less oxygen and carbon functional groups, reducing the chemical carbon consumption by 59.8% than H 2 SO 4 . The compressive strength reduces less due to its slight effect on the disordered graphitic structure. H 2 S also reacts with the C=O bond to form H 2 SO 3 or H 2 SO 4 . The desorption of H 2 SO 3 does not require carbon consumption. The decomposition of H 2 SO 4 needs to react with C=C bond to release SO 2 , CO 2 , and CO, and the compressive strength of activated carbon significantly decreases. The carbon consumption originates from two aspects, the one from the regeneration of sulfur-containing products is more than twice of the other one from the decomposition of oxygen-containing functional groups.

1. Introduction

Due to the leakage of coke oven gas from the furnace wall, coke oven flue gas contains approximately 200 mg/m^3 H_2S in addition to 150 mg/m^3 SO_2, and this issue must then be ameliorated by oxidation (Vinod and Tawfik, 2013). Activated carbon treatment of H_2S and SO_2 in flue gas is an environmentally friendly and effective purification technology (Braghiroli et al., 2019, Grzyb et al., 2009, Liu et al., 2003, Nguyen-Thanh et al., 2005, Rubio and Izquierdo, 2010). However, more than 20% of the operation cost per year is attributed to the supplement of activated carbon for activated carbon technology. The proportion of operation cost is calculated based on the coke oven flue gas purification project from ACRE Coking and Refractory Engineering Consulting Corporation in Hebei province, China. Therefore, the carbon consumption should be reduced for sustainable development and cleaner production.

Carbon consumption of activated carbon purification technology is obvious different under different industrial flue gas. For a long-term operation of activated carbon purification device, it is found that the carbon consumption in sintering flue gas purification is 1.15 ~ 1.2 times higher than that in coke oven flue gas purification. The both flue gas has a similar NO concentration about 300 ~ 400 ppm and total sulfur concentration about 200 ~ 300 ppm. While sintering flue gas only contains SO_2, but coke oven flue gas includes 30 ~ 50% H_2S except SO_2. Carbon consumption consists of physical carbon consumption and chemical carbon consumption. The main influencing factors of physical carbon consumption include the moving speed of activated carbon, wear resistance and compressive strength, which is no significant diversity between the two devices. The chemical carbon consumption is from the regeneration

of the sulfur-containing components. That is, the presence of H_2S may decrease the carbon consumption. At present, there is little research on the effects of H_2S on carbon consumption of activated carbon for flue gas purification.

Both H_2S and SO_2 in coke oven flue gas can cause sulfur species deposition on the activated carbon, which are usually treated by thermal regeneration to recover the reaction activity (Li et al., 2019a, Qi et al., 2014, Silas et al., 2018). SO_2 is combined with basic functional groups to generate H_2SO_4 (Guo et al., 2013, Karatepe et al., 2008, Xu et al., 2018). H_2S can be oxidized to sulfur, H_2SO_3 and H_2SO_4, which depend on the activated carbon surface properties and the atmosphere. H_2S associates with the oxygen functional groups on the activated carbon surface, producing H_2SO_4 and elemental sulfur. With O_2 in the atmosphere, H_2S can be oxidized to elemental sulfur, and then to produce gaseous SO_2 (Li et al., 2019a). In the thermal regeneration process, H_2SO_4 can react with activated carbon to release SO_2 and simultaneously produce CO and CO_2, which are the main sources of the chemical carbon consumption (Li et al., 2019b). H_2SO_3 decomposes at lower temperature, so its chemical carbon consumption is essentially negligible (Kim et al., 2019). Currently, the transformation of elemental sulfur in the regeneration process and its chemical carbon consumption are rarely studied. The physical carbon abrasion is related to the mechanical strength of the activated carbon as well as the moving speed of the activated carbon in the reactor. Regeneration will alter the lattice structure of the activated carbon and then affect its mechanical strength. To date, few studies have focused on this issue.

The adsorption products determine the carbon consumption at different degrees. Therefore, the deposition products of three typical sulfur-containing components were prepared on activated carbon in various adsorption atmospheres, and then the regeneration process was studied to elucidate the effect of sulfur containing substances on the physical structure and chemical characteristics of activated carbon. The sources of physical carbon abrasion and chemical carbon consumption were studied, and the strategy of reducing carbon consumption was put forward.

2. Material And Methods

2.1 Activated carbon preparation

The anthracite-based activated carbon (AC) is from Shanxi province. The material in the lab was pulverized, sieved to 20 - 60 mesh (0.25 - 0.85 mm), rinsed by deionized water, filtered and dried in a drying oven at 110 °C for 20 h; the activated carbon thus treated was marked as fresh AC. The fresh AC sample was pretreated in a fixed bed reactor with a diameter of 30 mm, with 1.50 ± 0.01 g sample charged, and then reacted with the mixture gas at a gas hourly space velocity of 5700 h^{-1} at 150 °C for 300 min. Four samples named blank sample and AC_1 - AC_3 were obtained in different gas: blank sample, N_2; AC_1, 50 ppm SO_2 and 150 ppm H_2S; AC_2, 200 ppm SO_2; AC_3, 200 ppm SO_2 and 5% O_2, with the balance N_2. The total molar contents of the sulfur substances, the adsorption time and the activated carbon used in the experiment were the same for the AC_1 - AC_3 samples.

2.2 Experimental conditions

The thermal regeneration process on the activated carbon samples was investigated in the above-mentioned fixed bed reactor. The regeneration process was carried out in N_2 and the gas flow rate was 180 ± 5 mL/min at a heating rate of 5 °C/min from 150 °C to the final temperature of 450 °C. The regenerated activated carbon was labeled as AC-re. The outlet concentration of the gas component was tested online by a Fourier transform infrared (FTIR) spectrometer (Tensor 27, Bruker, Germany). The integral area of the thermal regeneration curves could be used to calculate the CO and CO_2 contents with a minimum standard deviation of approximately 2%. And the same calculation method was also used for the temperature programmed desorption (TPD) curves obtained at a heating rate of 5 °C/min from 150 °C to 900 °C. Chemical carbon consumption referred to the sum of CO and CO_2 emitted per gram of activated carbon (mmol/g) during the regeneration.

2.3 Characterization methods

Elemental analysis was conducted using an Elemental Analyzer (Vario EL, Elementar, Germany). The C, N, H and S contents were characterized on the dry ash free (daf) basis of the AC samples with a minimum standard deviation of approximately 0.2%, and the O content was calculated by the difference method.

A simultaneous thermogravimetric (TG) analyzer (LABSYS EVO, SETARAM LABSYS, France) was used to test the TG and differential TG (DTG) curves over the 30 – 900 °C range at a heating rate of 5 °C/min in N_2. 50 mg analytically pure sulfur and 50 mg activated carbon were packed in a suprasil quartz glass tube, and heated in air.

The characterization methods of pore structure, graphite structure, X-ray photoelectron spectroscopy (XPS) and in situ diffuse reflectance infrared Fourier transform (DRIFT) spectra were represented in detail elsewhere (Fang et al., 2013, Li et al., 2018).

The electron paramagnetic resonance (ESR) spectra were measured to test the form of elemental sulfur on an X-band spectrometer (EMXplus-9.5/12, Bruker, USA) at room temperature, 150 °C and 400 °C.

Mechanical strength was measured using a compression strength tester (HNYQ6000, Huatong, China) and a wear resistance tester (MHXT-2D, Tianguan, China), that were customized according to the GB 30202.3-2013 standard. The average value was obtained after three tests with an error of 1% for wear resistance and 3% for compression strength.

3. Results And Discussion

3.1 Decomposition mechanism of sulfur products

To determine the differences in the sulfur-containing adsorption products, an elemental analysis of various AC samples was carried out, and the results are shown in Table 1. The sulfur contents of the AC_1 -

AC_3 samples are basically the same and significantly higher than that of the blank sample due to the strong adsorption capacity of activated carbon for H_2S and SO_2. For AC_1 - AC_3 samples, there is no clear difference in the sulfur and oxygen contents with a deviation of 2%. According to the previous study (Li et al., 2019a), the desulfurization efficiency of the three atmospheres used in the work can reach approximately 95% so that the sulfur contents of the three products are basically the same.

Table 1 Elemental composition of the activated carbon samples (wt%)

Samples	C	H	N	S	O
Fresh AC	79.10	1.19	0.99	0.34	18.38
Blank	79.27	1.31	1.02	0.44	17.96
AC_1	75.71	1.31	0.97	1.87	20.14
AC_2	76.15	1.13	1.07	1.79	19.78
AC_3	75.82	1.20	0.97	1.83	20.18

Fig. 1 shows the proportions of the elemental sulfur, SO_3^{2-} and SO_4^{2-} calculated from the data in Fig. S1. SO_4^{2-} and elemental sulfur (Liu et al., 2015, Menezes et al., 2018, Qiu et al., 2019) constitute the majority of sulfur products on the activated carbon surface for the four samples. The proportion of elemental sulfur in AC_1 is 65.8%, indicating that the oxidation products of H_2S are mostly elemental sulfur. AC_2 contains approximately 20.8% H_2SO_3, because H_2SO_3 can be formed by the reaction of SO_2 and H_2O in the atmosphere without O_2. However, due to the oxidation of oxygen-containing functional groups on the AC surface, H_2SO_3 will be oxidized to H_2SO_4 (Guo et al., 2013). The SO_4^{2-} content in AC_3 is greater than 60%, because SO_2 is adsorbed at the active site first and then is easily oxidized to H_2SO_4 in the presence of O_2.

According to the analysis of the elemental content and XPS spectra, the total sulfur content is basically the same for AC_1 - AC_3, and the difference lies in the forms of sulfur-containing products. The elemental sulfur accounts for the majority of the sulfur species in AC_1, while AC_2 contains 20.8% H_2SO_3, and the main sulfur product in AC_3 is H_2SO_4. The existence form of sulfur-containing products is determined by the adsorption atmosphere of different sulfur components with SO_2 and H_2S.

The XPS results of carbon and oxygen functional groups are shown in Table. S1 and S2. As shown in Fig. 2 (a), compared with the blank sample, the amount of C=C and C=O bonds of AC_1 clearly decrease, while the C-S bond increases. According to previous studies (Silas et al., 2018), in the process of H_2S oxidation, the C=C bond and C=O bond have been broken by H_2S, and then the C-S bond and S-O bond are generated as intermediate products. The C-S bond tends to form elemental sulfur, while the S-O bond is likely to form H_2SO_4. For the AC_2 and AC_3 samples, there is no clear change in the carbon functional

groups. After the thermal regeneration, the content of C-S bond in blank sample significantly decreases, due to the release of its own sulfur in the process of regeneration. The content of C=C bond basically changes little due to few sulfur compounds in the blank sample to react with C=C bond. For AC_1 - AC_3 samples, the main change is reflected in the reduction of C=C and C-S bonds, and the increase of the C=O and C-O bond. The C=C bond reacts with H_2SO_4 to release SO_2. The C-S bond is unstable and easily decomposes to release elemental sulfur at high temperature. The C=O and C-O bonds are more stable than the other carbon functional groups, so that the total amount of these two carbon functional groups changes little but their proportion increases. The decrease in the C=C bond is most obvious for AC_3, which is related to the fact that the highest H_2SO_4 content among the three samples is observed on AC_3.

As shown in Fig. 2 (b), compared with the blank sample, the C=O bond amount of AC_1 clearly decreases and the OH amount increases, due to the combination of the C=O bond with free H in H_2S. For AC_2 and AC_3, the OH amount obviously decreases, due to the form H_2SO_4 or H_2SO_3 through the combination of the OH site with SO_2. In the thermal regeneration process, COOH and OH can be decomposed below 450 °C and mainly from carboxyls, lactones and anhydrides (Vivovilches et al., 2014), which is an important reason for the loss of the carbon functional groups. While the C=O bond amount increases significantly, due to their stable chemical properties.

To further illustrate the decomposition process of the sulfur products in activated carbon, in situ DRIFT spectra are carried out with the results shown in Fig. 2 (c) and (d). H_2SO_3 (872 cm^{-1}) and H_2SO_4 (1090 cm^{-1}) are observed in the adsorption process, particularly for the AC_2 and AC_3 samples, but their amount decreases during the regeneration process. Due to the adsorption amount of acid SO_2, the alcohol (OH) (1240 cm^{-1}) decreases while alkyl ether (1020 cm^{-1}) increases in the AC_2 and AC_3 samples. In the regeneration process, the reduction of the S-O bond (1150 cm^{-1}) is most significant in AC_3, representing the decomposition of sulfuric acid. Another important change is the decomposition of carboxylic acid (1080 cm^{-1}). Carboxylic acid on the activated carbon surface decomposes below 450 °C, which is an important reason for the reduction in the denitrification efficiency of the activated carbon after regeneration.

In the regeneration process, the chemical carbon consumption comes from the decomposition of oxygen-containing functional groups and the reaction of activated carbon with H_2SO_4. Carboxyls, lactones and anhydrides with COOH and OH groups can be decomposed below 450 °C. The thermal decomposition of functional groups is independent with the type of sulfur-containing products. The thermal regeneration of sulfur-containing products results in the reduction of the C=C bond amount. The C=C bond reacts with H_2SO_4 to produce CO and CO_2.

3.2 Effect of sulfur products regeneration on chemical carbon consumption

Fig. 3 shows the SO_2 concentration for the AC_1 - AC_3 samples during the TPD process. The decomposition temperature range of H_2SO_3 is 150 ~ 300 °C, and H_2SO_4 decomposes at 300 ~ 450 °C

(Lin et al., 2018). Therefore, the regeneration temperature is set at 450 °C for the complete desorption of SO_2. At approximately 380 °C, a main peak of the H_2SO_4 decomposition is observed. A shoulder peak of SO_2 desorption is observed in AC_2 at 150 ~ 300 °C because the H_2SO_3 decomposition temperature is lower than that of H_2SO_4 (Kim et al., 2019). The peak areas of AC_1 - AC_3 in the range of 300 ~ 450 °C are 37523, 46112 and 67321, basically proportional to the H_2SO_4 contents of 33.1%, 39.7% and 60.7% calculated from the XPS spectra as given in Fig. 1. There are no clear differences between the total sulfur contents of the three adsorbed samples, while the concentration of the desorbed SO_2 from AC_1 is significantly lower than AC_2 and AC_3, indicating that the most of the sulfur in AC_1 decomposes in the form of elemental sulfur instead of SO_2.

Table 2 Elemental analysis of the activated carbon samples after the TPD process (wt%)

Samples	C	H	N	S	O
Blank	86.12	1.97	0.61	0.39	10.91
AC_1	86.16	1.67	1.09	0.44	10.64
AC_2	87.23	1.81	1.37	0.41	9.18
AC_3	88.02	1.77	1.01	0.52	8.68

The results of elemental analysis of various samples after the TPD process are shown in Table 2. Compared with the data in Table 1, the sulfur and oxygen contents in AC_1 - AC_3 samples decrease during the TPD process, due to the decomposition of the sulfur species and oxygen functional groups at high temperature (Lin et al., 2018). The sulfur content shows slight differences among the three samples, showing that the three samples have similar values of the total desorption amount of the sulfur species. However, clear differences among the three samples are observed for the oxygen content. The oxygen content of AC_1 is significantly higher than those of AC_2 and AC_3. It is inferred that the desorption process of elemental sulfur is different from that of H_2SO_4, with H_2SO_4 releasing more oxygen during the desorption process.

Fig. 4 show the results for the SO_2 desorption and chemical carbon consumption of the three samples during the regeneration process. The SO_2 desorption in AC_1 is much lower than that in AC_2 and AC_3, because the elemental sulfur desorption cannot be detected by FTIR. AC_1 has the smallest carbon consumption, because of the largest component of elemental sulfur. For AC_2, some H_2SO_3 can be decomposed directly at lower temperature, thus reducing the release of CO and CO_2. AC_3 consumes the most carbon, mainly due to the reaction of sulfuric acid and carbon.

The carbon consumption of blank sample can be used to calculate the decomposition of oxygen-containing functional groups during regeneration. As shown in Table 3, according to the comparison of the oxygen content between the activated carbon and blank sample, about 6% of the oxygen-containing

functional groups are consumed in the regeneration process. For AC_1, the total carbon consumption during regeneration is 0.28 mmol/g, of which 75% comes from the thermal decomposition of oxygen-containing functional groups and 25% originates from the reaction between C and H_2SO_4. For AC_3 sample, the total carbon consumption during regeneration is 0.68 mmol/g, including 31% from its own thermal decomposition and 69% from its reaction with H_2SO_4. The desorption of elemental sulfur consumes less oxygen and carbon functional groups, reducing the chemical carbon consumption by 59.8% than H_2SO_4. In AC_3, the carbon consumption caused by the regeneration of sulfur-containing products is more than twice of that caused by the decomposition of oxygen-containing functional groups, which indicates that the most important carbon consumption for the activated carbon used is caused by the reaction of C and H_2SO_4.

Table 3 SO_2 recovery and carbon consumption of the AC samples

Samples	S (mmol/g)		Carbon Consumption (mmol/g)			
	Adsorption (H_2S and SO_2)	Desorption (SO_2)	CO	CO_2	Total	C/S
blank	0	0	0.04	0.17	0.21	/
AC_1	0.76	0.15	0.06	0.22	0.28	0.45
AC_2	0.73	0.39	0.16	0.44	0.60	1.00
AC_3	0.77	0.36	0.20	0.48	0.68	1.12

* Blank refers to the blank activated carbon without adsorption.

Unlike H_2SO_4 and H_2SO_3, elemental sulfur cannot be determined during the desorption process. To further evaluate the morphology of sulfur products, DTG characteristics were used to measure the total weight loss at various temperature ranges, with the results shown in Fig. 5. The peak at 350 °C represents the decomposition of H_2SO_4, while elemental sulfur directly sublimates at approximately 380 °C. Based on the temperature peak position, AC_1 mainly contains elemental sulfur and a small amount of H_2SO_4, and AC_2 contains less H_2SO_4 than AC_3. H_2SO_4 and a small amount of elemental sulfur are found on the surface of AC_3. The differences between the peak area of DTG curves and that of SO_2, CO and CO_2 content curves are the content of elemental sulfur. And elemental sulfur in AC_1 is the highest, which is consistent with the results in Fig. 1. It can be concluded from the DTG curves that the elemental sulfur sublimates at 350 ~ 400 °C, which is of great significance to guide the design for industrial flue gas purification by activated carbon process.

Electron Spin Resonance was used to calculate the average chain length of sulfur by dividing the number of electron spin (Terada et al., 2020). The ESR spectrogram is shown in Fig. S3.

$$L = \left(\frac{\frac{1}{100}}{32.07} \times N_A\right)/\left(E \times \frac{1}{2}\right) \qquad \text{Equation (1)}$$

Where E (in spins per gram) is the amount of electron spin of samples, N_A (6.022×10^{23} mol^{-1}) is Avogadro constant. It is difficult to test the electron spin of activated carbon because of its magnetism. So, the results of elemental sulfur were used to characterize the properties of elemental sulfur produced by adsorption on activated carbon, as shown in Fig.6. When the elemental sulfur rises from room temperature to 150 ℃, the chain length of sulfur has no obvious change, and the average value is about 2×10^6. It is difficult for orthorhombic sulfur to exist at 150 ℃, the sulfur form at this temperature is monoclinic sulfur (S_8) (Terada et al., 2020). Each sulfur atom forms covalent single bond with the other two sulfur atoms in sp^3 hybrid orbit (Brandi et al., 2019). When the temperature continues to rise up to 254 ℃, the electron spin number of sulfur is close to 0, the S_8 ring structure breaks into infinitely long chain molecules (S_∞) which are twisted back together. The temperature continues to rise to 400 ℃, the average chain length of sulfur decreases to 0.7×10^6, the sulfur becomes vapor, and there are S_8, S_6, S_2 and other molecules in the vapor (Lau et al., 2017).

For the composition of sulfur vapor, the energy barriers of $\cdot S_2 \cdot$ and $\cdot S_6 \cdot$ are only 209.45 kJ/mol (Song et al., 2019). It is the lowest energy barriers of the ring opening reaction of S_8, which indicates that the reaction is easy to occur when the S_8 chain breaks. The energy barrier of $\cdot S_4 \cdot$ is 447.07 kJ/mol (Jones and Ballone, 2003), which is difficult to occur. Therefore, only three products of S_2, S_6, S_8 are calculated when calculating the equilibrium sulfur vapor products. According to principle of minimum free energy (Catone et al., 2019), the volume fraction of each component for sulfur vapor at 400 ℃ is 3.7% for S_2， 56.4% for S_6 and 39.9% for S_8. At the adsorption temperature, the state of elemental sulfur is monoclinic sulfur, which is composed of S_8 ring molecules. When the activated carbon is regenerated, the temperature rise first causes the S_8 ring structure to break into infinitely long chain molecules (S_∞). Above 254 ℃, the long chain sulfur breaks into small molecules, such as S_6 and S_2. At 400 ℃, the sulfur becomes vapor, and the volume fraction of each component for sulfur vapor is 3.7% for S_2, 56.4% for S_6 and 39.9% for S_8.

Table 4 shows the reactions of sulfur-containing substances with activated carbon in the adsorption-regeneration process. C(O) represents the oxygen functional groups on the activated carbon surface.

Table 4 Reactions for adsorption-regeneration process of sulfur-containing substances on activated carbon

Process	Change of reactants	Reaction	Participating functional groups	No.
Adsorption	Adsorption and oxidation of SO_2	$SO_2 \rightarrow H_2SO_3$	OH	(1)
		$SO_2 \rightarrow H_2SO_4$		(2)
	Oxidation of H_2S	$H_2S \rightarrow S(s)$	Reactant: C=O, C=C Intermediate product: C-S, S-O	(3)
		$H_2S \rightarrow H_2SO_3$		(4)
		$H_2S \rightarrow H_2SO_4$		(5)
Regeneration	Regeneration of sulfur products	$H_2SO_4+C \rightarrow SO_2+CO+H_2O$	C=C	(6)
		$2H_2SO_4+2C \rightarrow 2SO_2+CO_2+2H_2O$		(7)
		$H_2SO_3 \rightarrow SO_2+H_2O$		(8)
		$S(s) \rightarrow S(g)$		(9)
	Decomposition of carbon-functional groups	$C(O) \rightarrow CO_2$	carboxyls, lactones and anhydrides	(10)
		$C(O) \rightarrow CO$		(11)

The carbon consumption partly depends on the existence form of sulfur-containing products, in addition to the thermal decomposition of functional groups. The desorption of elemental sulfur consumes less oxygen and carbon functional groups, with 59.8% less chemical carbon consumption than H_2SO_4. The carbon consumption caused by the regeneration of sulfur-containing products is less than that by the decomposition of functional groups with elemental sulfur as the main products.

3.3 Influence of sulfur products regeneration on physical carbon abrasion

To investigate the influence of sulfur products regeneration on the AC physical structure, the pore structures were analyzed before and after the regeneration. The results are shown in Table 5. In comparison with the blank sample, the specific surface area and pore volume of AC_1 - AC_3 clearly decrease due to the sediment of sulfur substances on the activated carbon surface. Moreover, the specific surface area of AC_1 decreases by 11% and that of AC_3 decreases by 20%. This phenomenon is ascribed to the different volumes of elemental sulfur and H_2SO_4. The volume of elemental sulfur is 13.6 cm^3/mol, while that of sulfuric acid is 53.5 cm^3/mol, and that of H_2SO_3 is 79.6 cm^3/mol (Lau et al., 2017). Therefore, when elemental sulfur rather than H_2SO_4 is deposited on the activated carbon surface, the decrease in the specific surface area is not obvious. After thermal regeneration, both the specific surface area and pore volume increase because of the partial decomposition of the functional groups. The pore

size of the activated carbon is restored to the level of the fresh activated carbon, and even increases after the regeneration.

Table 5 Characterization of the various AC before and after regeneration

Sample	S_{BET} (m^2/g)		V_m (mL/g)		V_t (mL/g)	
	Be-re	Af- re	Be- re	Af-re	Be- re	Af-re
Fresh AC	196		0.070		0.087	
Blank	198	221	0.070	0.070	0.091	0.096
AC_1	175	215	0.065	0.073	0.076	0.096
AC_2	161	200	0.059	0.070	0.076	0.093
AC_3	157	199	0.059	0.070	0.069	0.093

*Be-re is the abbreviation of before-regeneration. Af-re is the abbreviation of after-regeneration.

The graphite microcrystalline structure of the AC samples before and after regeneration was shown in Fig. 7. Raman spectra of all samples displays two peaks including the disorder (D) peak at 1360 cm^{-1} reflecting the structural defects and the graphite (G) peak at 1600 cm^{-1} reflecting the sp^2 carbon atoms in the graphene sidewalls. The ratio of the peak intensity (I_D/I_G) represents the degree of disorder in the graphite microcrystalline structure on activated carbon (Zhang et al., 2019). The D and G peaks of various AC samples are basically the same prior to regeneration. The D peaks of AC_1 - AC_3 samples clearly increase after regeneration, while the G peak does not change much, so that the I_D / I_G value increases significantly, particularly for AC_3. This indicates that regeneration can significantly improve the disorder in the activated carbon.

From the macroscopic point of view, the activated carbon structure can also be characterized by compressive strength and wear resistance, which are tested before and after regeneration, with results shown in Fig. 8. There is little difference between the wear resistance values before and after regeneration, while the compressive strength clearly decreases, especially for the AC_2 and AC_3 samples, indicating that the reaction of C and H_2SO_4 destroys the integrity of the carbon structure. The compressive strength and wear resistance decrease on regenerated activated carbon, leading to the increase in the amount of small granular activated carbon, and finally increase the physical carbon abrasion.

3.4 Total carbon consumption in engineering applications

The total carbon consumption in engineering applications includes chemical carbon consumption and physical carbon abrasion. In this work, two factories using activated carbon technology for flue gas purification were investigated. One is for sintering flue gas purification to capture SO_2, and the other is for coke oven flue gas purification to simultaneously remove SO_2 and H_2S. The results are shown in Table 6.

For sintering flue gas purification, the total carbon consumption is about 55% of the total charge per year; among them, the physical carbon abrasion is about 38%, and the chemical carbon consumption is about 17%. The physical carbon abrasion is twice more than chemical carbon consumption. The total carbon consumption is approximately 48% for coke oven flue gas, lower than that for sintering flue gas. The high content of H_2S depresses the carbon consumption in the regeneration process compared with the same content of SO_2.

Table 6 Comparison of total carbon consumption between sintering flue gas and coke oven flue gas

	Sintering flue gas	Coke oven flue gas
Total gas volume (Nm^3/h)	2,800,000	300,000
Inlet SO_2 (ppm)	200~300	50~100
Inlet H_2S (ppm)	/	150~200
Outlet SO_2 (ppm)	20	10
Outlet H_2S (ppm)	/	15
Total AC loading (t)	12,000	2500
Total AC consumption (t/a)	6600	1200
Physical carbon abrasion	38%	35%
Chemical carbon consumption	17%	13%

In order to reduce carbon consumption, the following strategies can be considered. Use air screen sorting devices to reduce physical carbon abrasion. With the increase of operation time, the particle size of activated carbon becomes smaller and smaller. The small particles and dust fill in the gap of activated carbon bed increasing the resistance of flue gas. An efficient balance vibrating screen in the activated carbon conveying system is commonly used to screen out small particles, but this measure will undoubtedly greatly increase the physical carbon abrasion between the particles and particle with vibrating screen. In order to solve this problem, an air screen sorting device for activated carbon was developed in the project. Driven by the upstream hot air flow, the dust and small particles in the activated carbon were gradually fluidized, suspended, and finally separated under the traction of the upstream air flow. This process reduces the collision and friction between the particles and vibrating screen, and then greatly reduces the physical carbon abrasion.

Select a high-quality activated carbon to reduce chemical carbon consumption. In engineering, the main quality index of activated carbon includes sulfur capacity, wear resistance, compressive strength, ignition point, and particle size distribution etc. In this work, it is found that elemental sulfur generated by H_2S can reduce the chemical carbon consumption of activated carbon. Therefore, the activated carbon with less C=O bond should be selected under the premise of ensuring the above quality index, which can effectively reduce the production of H_2SO_4 and greatly reduces the chemical carbon consumption.

4. Conclusions

H_2S can react with the C=C bond on the activated carbon surface to form C-S bond as an intermediate state, followed by the formation of elemental sulfur. It directly sublimates at approximately 380 °C, about 30 °C higher than the decomposition temperature of H_2SO_4. So, the regeneration temperature should be determined according to the sublimation temperature of elemental sulfur in the engineering application. At the adsorption temperature, the state of elemental sulfur is monoclinic sulfur in the form of S_8 ring molecules. When the activated carbon is regenerated, the temperature rise first causes the S_8 ring structure to break into infinitely long chain molecules (S_∞). When the activated carbon is heated above 254 °C, the long chain sulfur breaks into small molecules. At 400 °C, the sulfur becomes vapor, and the volume fraction of each component for sulfur vapor is 3.7% for S_2, 56.4% for S_6 and 39.9% for S_8. The desorption process of elemental sulfur consumes less oxygen and carbon functional groups, reducing the chemical carbon consumption by 59.8% than H_2SO_4; due to the slight effect on the disordered graphitic structure, its compressive strength is reduced less.

H_2S also reacts with the C=O bond to form H_2SO_3 and H_2SO_4. The decomposition of H_2SO_3 does not require carbon consumption. The deposited H_2SO_4 reacts with the C=C bond to generate SO_2, which is the cardinal reaction of the thermal regeneration. In addition, H_2SO_4 decomposition improves the ratio of the disordered graphitic structure. About 6% of the oxygen-containing functional groups are consumed in the regeneration process, and most of these functional groups are carboxyls, lactones and anhydrides. The carbon consumption caused by the regeneration of sulfur-containing products is more than that caused by the decomposition of oxygen-containing functional groups.

From the data of engineering project, the total carbon consumption of coke oven flue gas is slightly lower than that of sintering flue gas. H_2S will depress the carbon consumption in the thermal regeneration process compared with SO_2. To reduce carbon consumption, the following two strategies can be considered. Use air screen sorting devices to reduce the collision between activated carbon and vibrating screen, and then significantly reduces the physical carbon abrasion. Select the activated carbon with less C=O bond to reduce the production of H_2SO_4, and then greatly reduce the chemical carbon consumption.

Declarations

Ethics approval and consent to participate: This manuscript has been developed in compliance with ethical standards.

Consent for publication: This manuscript does not contain data from any individual person.

Availability of data and materials: The datasets used and/or analysed during the current study are available from the corresponding author on reasonable request.

Consent to participate: The authors voluntarily agreed to participate in this research study.

Consent to publish: The authors agree to publish the article in the Environmental Science and Pollution Research.

Competing interests: The authors declare that they have no competing interests.

Funding: This work was supported by the National Key Research and Development Program of China (No. 2017YFC0210600) and the National Natural Science Foundation of China (No. U1810209). The role of the funding body is in the design of the study, analysis, and interpretation of data.

Authors Contributions:

Yuting Lin: Conceptualization, Methodology, Formal analysis, Writing- Original draft preparation.

Yuran Li.: Resources, Writing - Review & Editing.

Zhicheng Xu: Visualization, Investigation.

Junxiang Guo: Supervision.

Tingyu Zhu: Resources, Supervision.

Acknowledgments: This work was supported by the National Key Research and Development Program of China (No. 2017YFC0210600) and the National Natural Science Foundation of China (No. U1810209).

References

Braghiroli F L, Bouafif H, Koubaa A. Enhanced SO_2 adsorption and desorption on chemically and physically activated biochar made from wood residues [J]. *Industrial Crops and Products*, 2019, 138:1803–1808. https://doi.org/ 10.1016/j.indcrop.2019.06.019

Brandi Cron, Pauline Henri, Clara S. Chan, et al. Elemental Sulfur Formation by Sulfuricurvum kujiense Is Mediated by Extracellular Organic Compounds [J]. *Original Research Article*, 2019, 10:2710-2717. https://doi.org/10.3389/fmicb.2019.02710

Catone D, Satta M, Cartoni A, et al. Gas Phase Oxidation of Carbon Monoxide by Sulfur Dioxide Radical Cation: Reaction Dynamics and Kinetic Trend with the Temperature [J]. Frontiers in Chemistry, 2019, 7:140. https://doi.org/ 10.3389/fchem.2019.00140

Fang H B, Zhao J T, Fang Y T, et al. Selective oxidation of hydrogen sulfide to sulfur over activated carbon-supported metal oxides [J]. *Fuel*, 2013, 108:143-148. https://doi.org/10.1016/j.fuel.2011.05.030

Guo Y, Li Y, Zhu T, et al. Effects of Concentration and Adsorption Product on the Adsorption of SO2 and NO on Activated Carbon [J]. Energy & Fuels, 2013, 27(1):360-366. https://doi.org/ 10.1021/ef3016975

Grzyb B, Albiniak A, Broniek E, et al. SO_2 adsorptive properties of activated carbons prepared from polyacrylonitrile and its blends with coal-tar pitch [J]. *Microporous and Mesoporous Materials*, 2009, 118(1-3):163-168. https://doi.org/ 10.1016/j.micromeso.2008.08.032

Jones G J, Ballone P. Density functional and Monte Carlo studies of sulfur: I. Structure and bonding in S_n clusters (n=2-18) [J]. *Journal of Chemical Physics*, 2003, 118(20): 9257-9265. https://doi.org/10.1063/1.1568081

Karatepe N., Orbak İ., Yavuz R., Özyuğuran A. Sulfur Dioxide Adsorption by Activated Carbons Having Different Textural and Chemical Properties [J]. *Fuel*, 2008, 54:324-331. https://doi.org/ 10.1016/j.fuel.2008.06.002

Kim J, Lee S, Kwon D W, et al. SO_3^{2-}/SO_4^{2-} functionalization-tailorable catalytic surface features of Sb-promoted $Cu_3V_2O_8$ on TiO_2 for selective catalytic reduction of NO_x with NH_3 [J]. *Applied Catalysis A: General*, 2019, 570:355-366. https://doi.org/ 10.1016/j.apcata.2018.11.024

Lau G E, Cosmidis J, Grasby S E, et al. Low-temperature formation and stabilization of rare allotropes of cyclooctasulfur (β-S_8 and γ-S_8) in the presence of organic carbon at a sulfur-rich glacial site in the Canadian High Arctic [J]. *Geochimica Et Cosmochimica Acta*, 2017, 200:218-231. https://doi.org/10.1016/j.gca.2016.11.036

Li K, Liu S, Song X, et al. Catalytic Oxidation of Hydrogen Sulfide on Fe/WSAC Catalyst Surface Modification via NH_3-NTP: Influence of Gas Gap and Dielectric Thickness [J]. *Industrial & Engineering Chemistry Research*, 2018, 57(8):2873-2881. https://doi.org/ 10.1021/acs.iecr.7b05079

Li Y, Lin Y, Xu Z, et al. Oxidation mechanisms of H_2S by oxygen and oxygen-containing functional groups on activated carbon [J]. *Fuel Processing Technology*, 2019, 189:110-119. https://doi.org/ 10.1016/j.fuproc.2019.03.006

Li Y, Lin Y, Wang B, et al. Carbon consumption of activated coke in the thermal regeneration process for flue gas desulfurization and denitrification [J]. *Journal of Cleaner Production*, 2019, 228:1391-1400. https://doi.org/ 10.1016/j.jclepro.2019.04.225

Lin Y, Li Y, Xu Z, et al. Transformation of functional groups in the reduction of NO with NH_3 over nitrogen-enriched activated carbons [J]. *Fuel*, 2018, 223:312-323. https://doi.org/ 10.1016/j.fuel.2018.01.092

Liu Q, Guan J S, Li J, et al. SO_2 removal from flue gas by activated semi-cokes: 2. Effects of physical structures and chemical properties on SO_2 removal activity [J]. *Carbon*, 2003, 41(12):2225–2230. https://doi.org/ 10.1016/S0008-6223(03)00230-6

Liu T, Xue L, Guo X. Study of Hg^0 removal characteristics on Fe_2O_3 with H_2S [J]. *Fuel*, 2015, 160:189-195. https://doi.org/ 10.1016/j.fuel.2015.07.093

Menezes R L C B, Moura K O, Sebastião M. P. de Lucena, et al. Insights on the Mechanisms of H_2S Retention at Low Concentration on Impregnated Carbons[J]. *Industrial & Engineering Chemistry Research*, 2018, 57(6). https://doi.org/ 10.1021/acs.iecr.7b03402

Nguyen-Thanh D, Bandosz T. J, et al. Activated carbons with metal containing bentonite binders as adsorbents of hydrogen sulfide [J]. *Carbon*, 2005, 43(2):359-367. https://doi.org/ 10.1016/j.carbon.2004.09.023

Qi J, Chen S, Cui X, et al. High Surface Area Nitrogen-Containing Porous Carbon Synthesis and Adsorption of Pb (II) and Cr (VI) Ions [J]. *Science of Advanced Materials*, 2014., 6: 963-969. https://doi.org/ 10.1166/sam.2014.1860

Qiu T, Nie Q, He Y, et al. Density functional theory study of cyanide adsorption on the sphalerite (110) surface [J]. *Applied Surface Science*, 2019, 465:678-685. https://doi.org/ 10.1016/j.apsusc.2018.09.020

Rubio B, Izquierdo M T. Coal fly ash based carbons for SO_2 removal from flue gases[J]. *Waste Management*, 2010, 30(7):1341-1347. https://doi.org/ 10.1016/j.wasman.2010.01.035

Silas K, Ghani W, Choong T, Rashid U. Activated carbon monolith Co_3O_4 based catalyst: Synthesis, characterization and adsorption studies [J]. *Environmental Technology & Innovation*, 2018, 12:273-285. https://doi.org/ 10.1016/j.eti.2018.10.008

Song X, Sun L, Guo H, et al. Experimental and Theoretical Studies on the Influence of Carrier Gas for COS Catalytic Hydrolysis over MgAlCe Composite Oxides [J]. *ACS Omega*, 2019, 4(4):7122-7127. https://doi.org/ 10.1021/acsomega.9b00517

Terada Naoki, Kouge Katsushige, Komaguchi Kenji, et al. Thermal Stability Change of Insoluble Sulfur by a Heat Treatment and Its Mechanism Study [J]. *Analytical Sciences*, 2020, 36:75-79. https://doi.org/ 10.2116/analsci.19SAP05

Vinod G, Tawfik S. Sorption of pollutants by porous carbon, carbon nanotubes and fullerene-An overview [J]. *Environmental Science & Pollution Research*, 2013, 20(5):2828-2843. https://doi.org/ 10.1007/s11356-013-1524-1

Vivovilches J F, BailónGarcía, Esther, PérezCadenas, Agustín F, et al. Tailoring the surface chemistry and porosity of activated carbons: Evidence of reorganization and mobility of oxygenated surface groups [J]. *Carbon*, 2014, 68(3):520-530. https://doi.org/ 10.1016/j.carbon.2013.11.030

Xu J, Chen G, Guo F, et al. Development of wide-temperature vanadium-based catalysts for selective catalytic reducing of NO_x with ammonia: Review [J]. *Chemical Engineering Journal*, 2018, 353:507-518. https://doi.org/ 10.1016/j.cej.2018.05.047

Zhang H, Li S, Jiao Y, et al. Structure, surface and reactivity of activated carbon: From model soot to Bio Diesel soot [J]. *Fuel*, 2019, 257:324-331. https://doi.org/ 10.1016/j.fuel.2019.116038

Figures

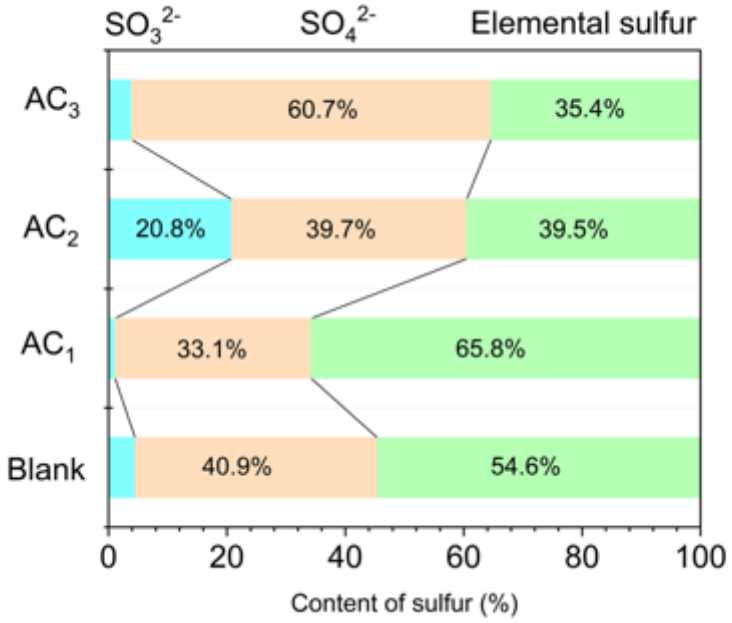

Figure 1

S 2p peaks from XPS for the activated carbon samples

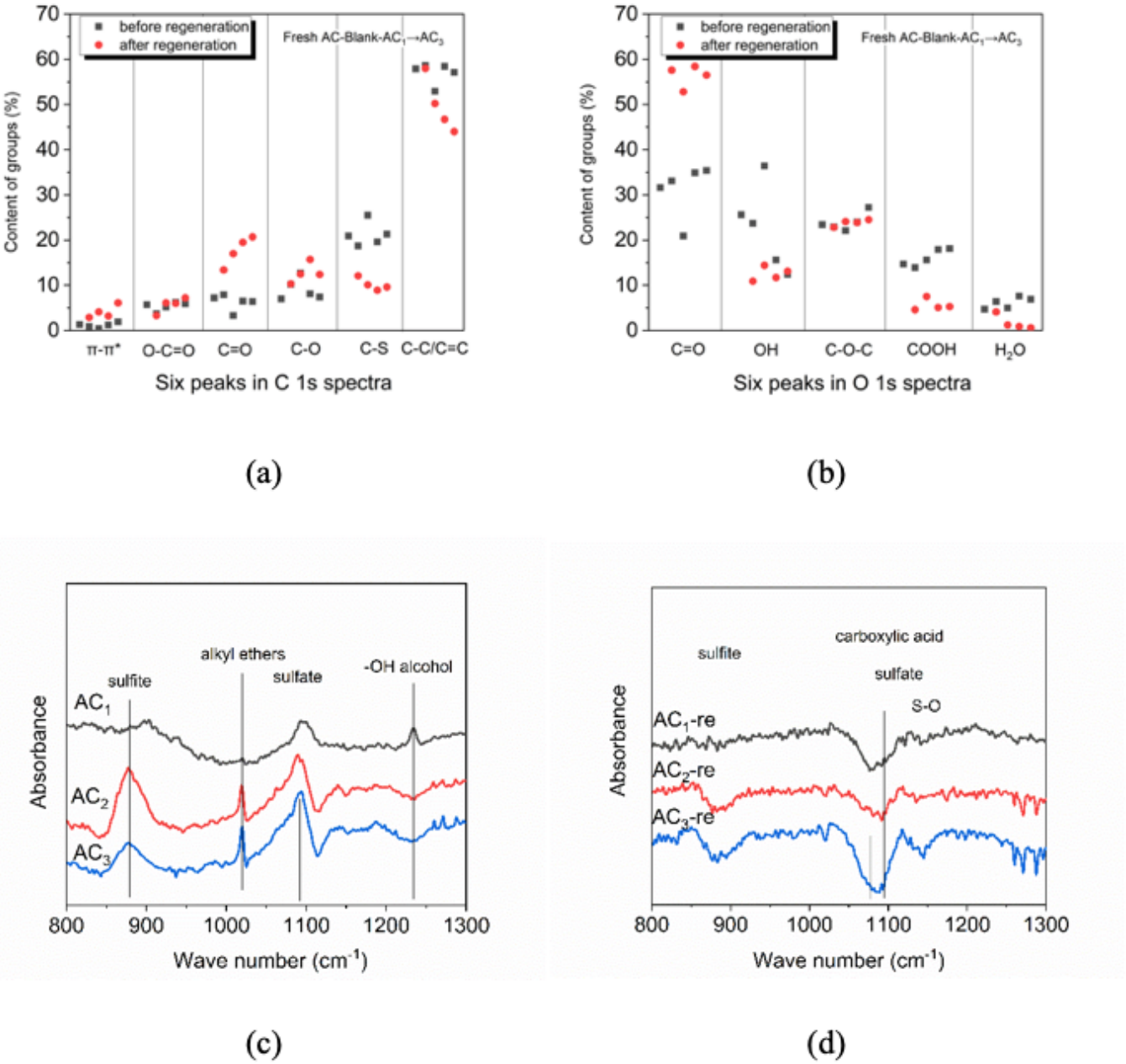

Figure 2

Content of carbon (a) and oxygen functional groups (b) in the samples in situ DRIFT spectra of the samples before (c) and after (d) regeneration

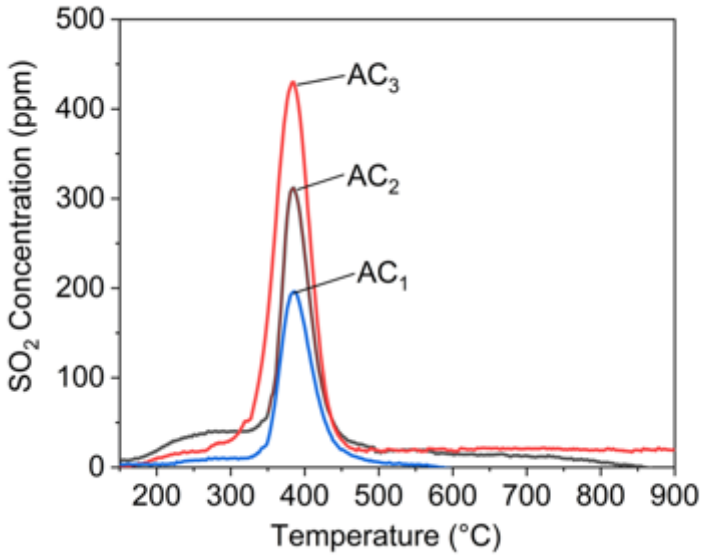

Figure 3

SO2 concentration during the TPD process for the activated carbon samples

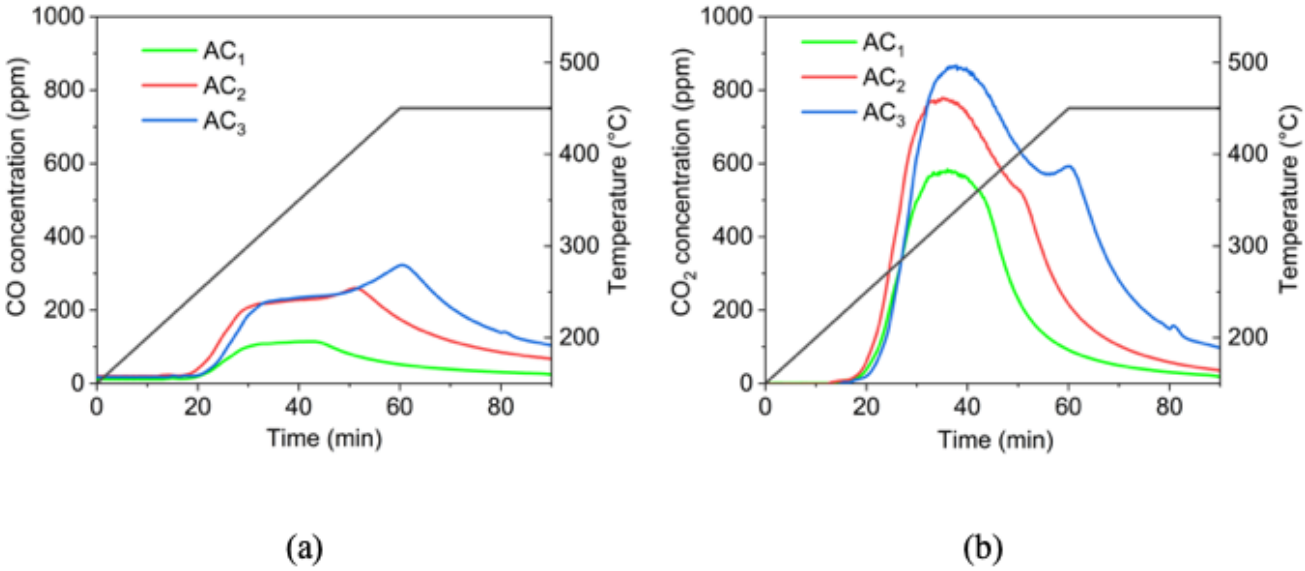

Figure 4

CO (a) and CO2 (b) concentration during the regeneration process

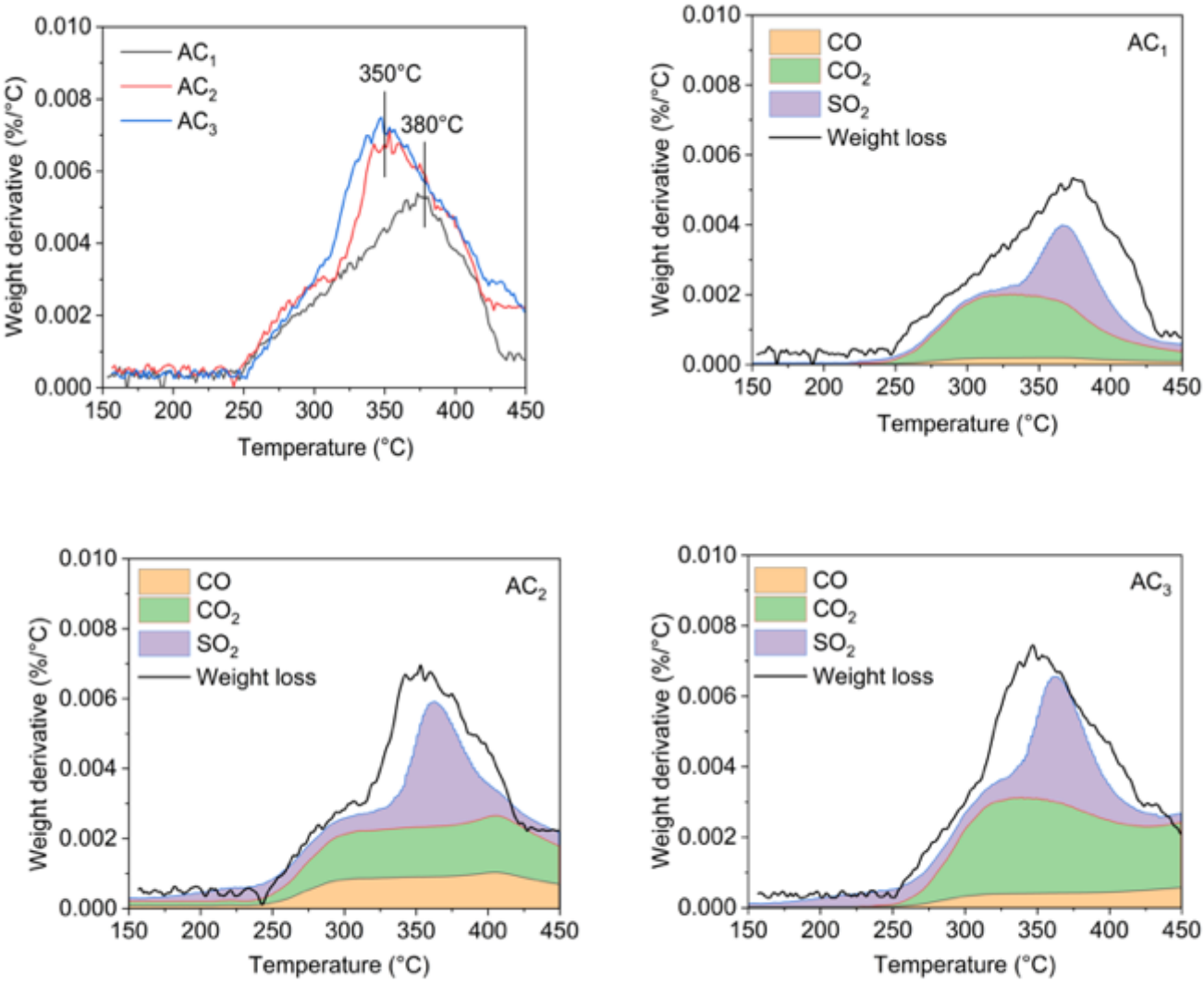

Figure 5

DTG curves for the absorbed AC

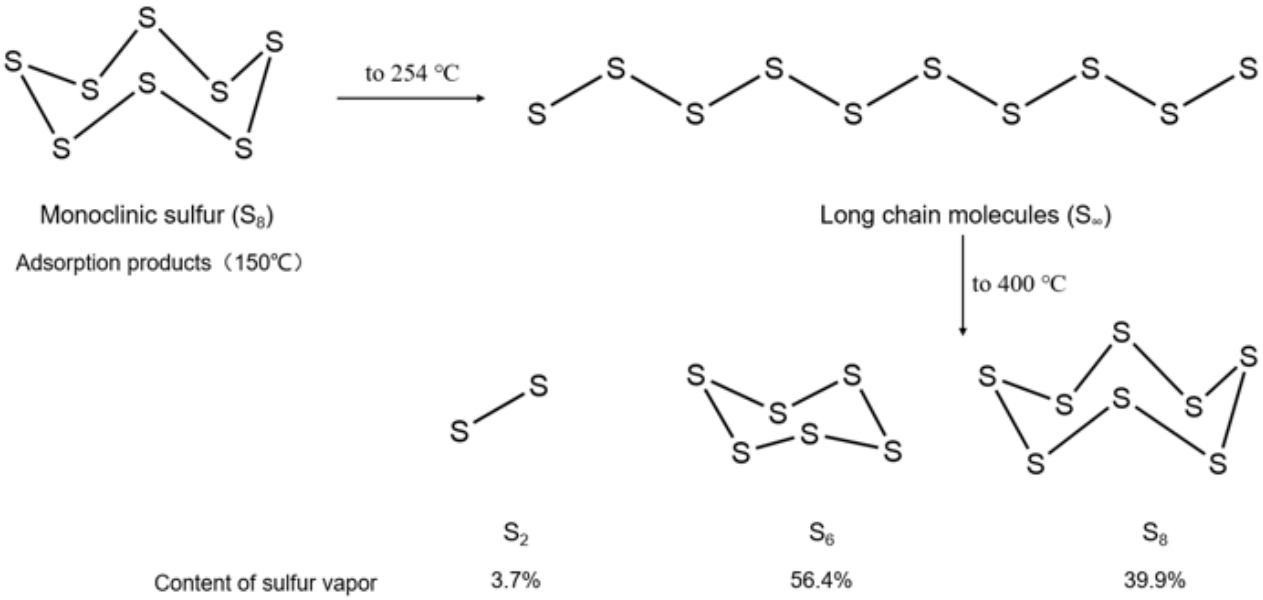

Figure 6

Morphological changes of elemental sulfur during adsorption-regeneration process

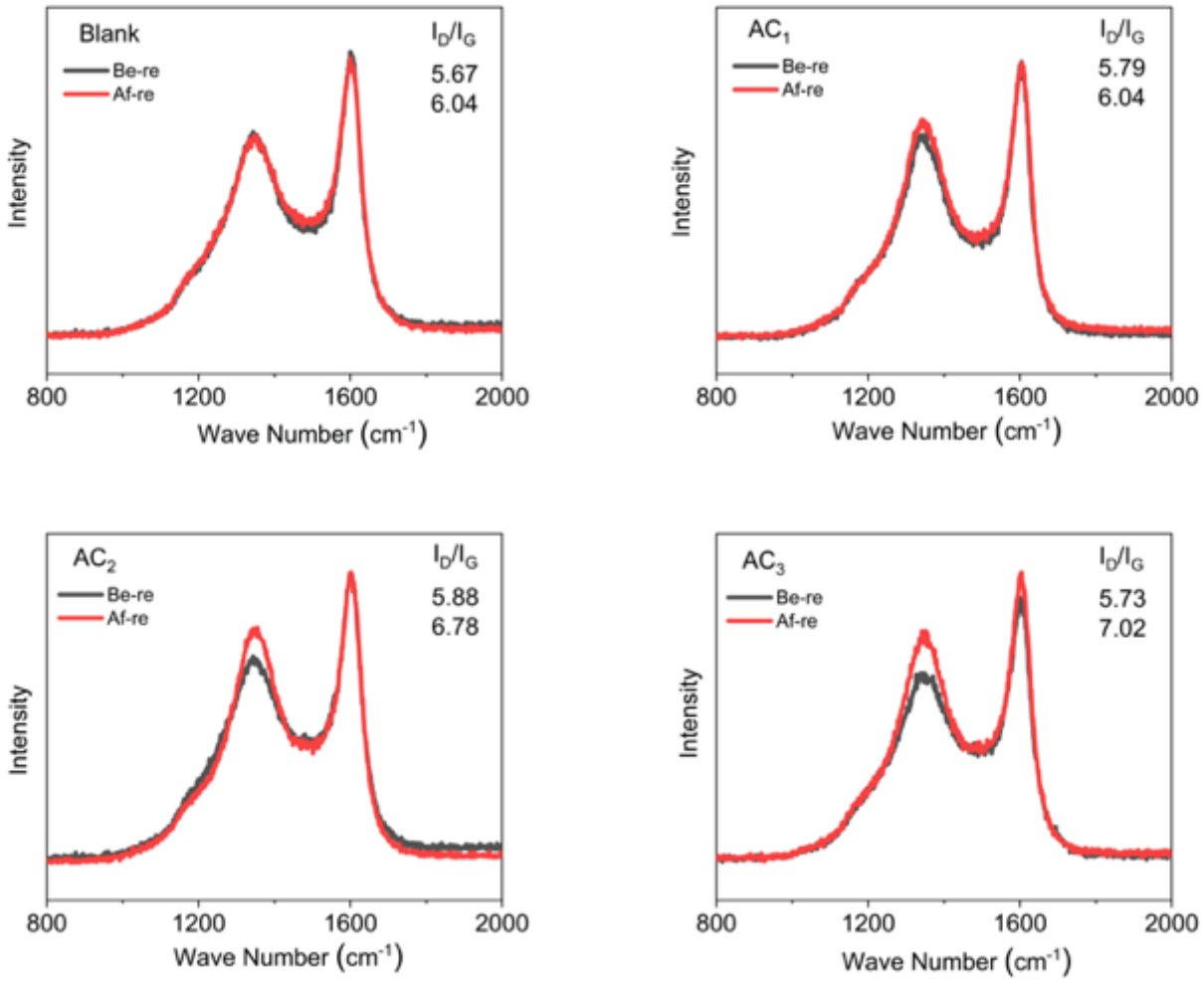

Figure 7

Raman spectra for various AC samples before and after regeneration

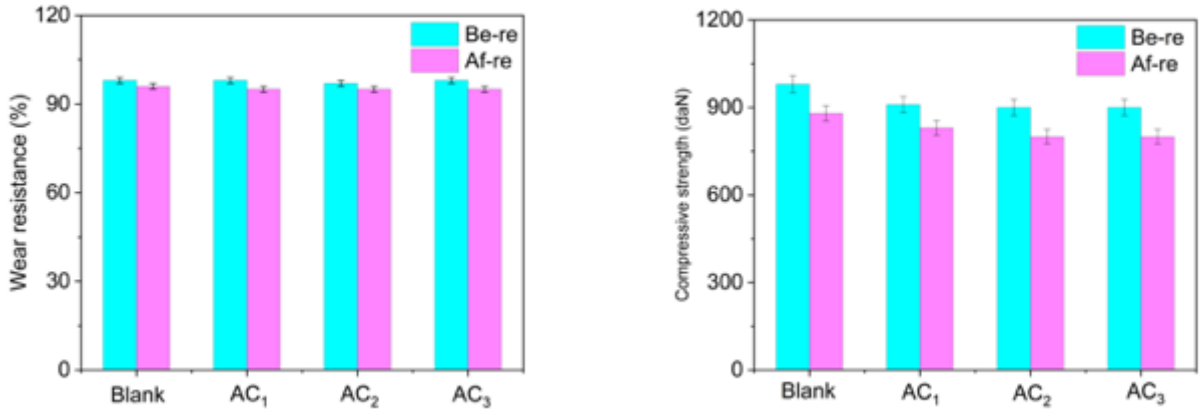

Figure 8

Wear resistance and compressive strength of the AC samples before and after regeneration *Be-re is the abbreviation of before-regeneration. Af-re is the abbreviation of after-regeneration.

Supplementary Files

This is a list of supplementary files associated with this preprint. Click to download.

- Graphicsummary.tif
- supportinginformation.docx